Feature-preserving Artifact Removal from Dermoscopy Images

Howard Zhou[a], Mei Chen[b], Richard Gass[b], James M. Rehg[a]

Laura Ferris[c], Jonhan Ho[c], Laura Drogowski[c]

[a]School of Interactive Computing, Georgia Tech, 85 5th Street NW Atlanta, GA 30332, USA
[b]Intel Research Pittsburgh, 4720 Forbes Avenue, Suite 410 Pittsburgh, PA 15213, USA
[c]University of Pittsburgh Medical Center, 580 S. Aiken Avenue, PA 15232, USA

ABSTRACT

Dermoscopy, also called surface microscopy, is a non-invasive imaging procedure developed for early screening of skin cancer. With recent advance in skin imaging technologies and image processing techniques, there has been increasing interest in computer-aided diagnosis of skin cancer from dermoscopy images. Such diagnosis requires the identification of over one hundred cutaneous morphological features. However, computer procedures designed for extracting and classifying these intricate features can be distracted by the presence of artifacts like hair, ruler markings, and air bubbles. Therefore, reliable artifact removal is an important pre-processing step for improving the performance of computer-aided diagnosis of skin cancer. In this paper, we present a new scheme that automatically detects and removes hairs and ruler markings from dermoscopy images. Moreover, our method also addresses the issue of preserving morphological features during artifact removal. The key components of this method include explicit curvilinear structure detection and modeling, as well as feature guided exemplar-based inpainting. We experiment on a number of dermoscopy images and demonstrate that our method produces superior results compared to existing techniques.

Keywords: dermoscopy, artifact removal, image restoration and enhancement, skin cancer, surface microscopy

1. INTRODUCTION

Skin cancer is the most common form of malignancy occurring in humans and it can be categorized into melanoma and non-melanoma. In the United States, the incidence of melanoma is growing at a rate greater than any other form of cancer.[1] It is also the leading cause of mortality among all forms of skin cancer. Nevertheless, melanoma can often be cured with a simple excision if caught in early stage. Hence, early detection of malignant melanoma significantly reduces mortality. Dermoscopy is a noninvasive imaging technique that has been shown effective for such a purpose. The procedure involves using an incident light magnification system, i.e. a dermatoscope, to examine skin lesions. Often oil is applied at the skin-microscope interface. This allows the incident light to penetrate the top layer of the skin tissue and reveal the pigmented structures beyond what would be visible by naked eyes. Dermoscopy has been shown to improve the diagnostic accuracy of dermatologists by as much as 30% over clinical examination.[1]

When acquiring dermoscopy images for computer-aided diagnosis, the practitioners mount cameras on the back of dermatoscopes, taking pictures as they exam the patients. A typical examining session only lasts several minutes. As a result of the time constraint, some common artifacts such as hair and air bubbles often appear in the acquired images. The presence of such artifacts can interfere with many analytic procedures required for accurate diagnosis, as illustrated in Fig. 1. In the first example (Fig. 1(a)), the segmentation algorithm presented in Grana *et al.*[2] mistakes a piece of hair (indicated by the arrows) as the lesion boundary. In Fig. 1(b), the hair at the top of the image confuses the same network analysis procedure[2] and masquerades as part of the pigmented network. Similarly in Fig. 1(c), hairs break the network pattern extracted by a similar procedure developed by Fleming *et al.*[3]

Further author information: (Send correspondence to Howard Zhou)
Howard Zhou: E-mail: howardz@cc.gatech.edu, Telephone: 1 404 385 4228

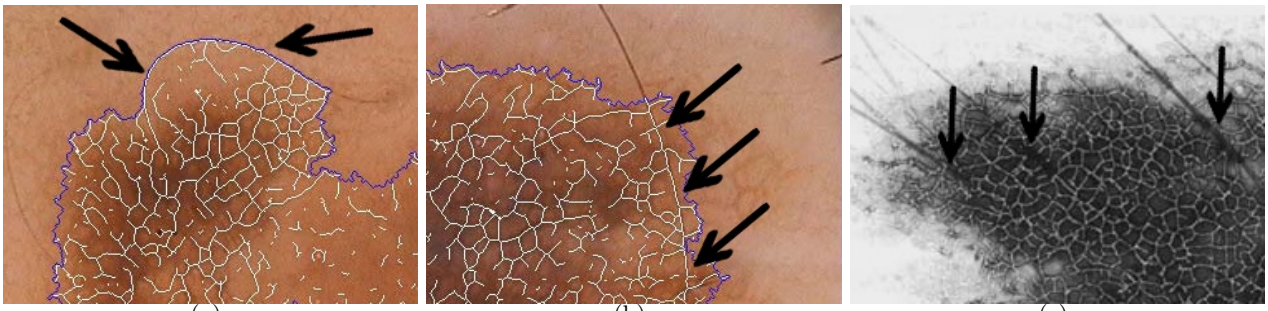

(a) (b) (c)

Figure 1. Artifacts interfering with computer procedures designed to extract dermoscopic features. (a) Hair affecting lesion segmentation (image courtesy of Grana *et al.*). (b) Hair masquerading as pigmented network (image courtesy of Grana *et al.*). (c) Hair interfering with pigmented network extraction (image courtesy of Fleming *et al.*).

Therefore, removal of such artifacts is an important prerequisite for accurate computed-aided diagnosis of pigmented skin lesions. Previous efforts in artifact removal from dermoscopy images include the works of Schmid *et al.*[4] and Fleming *et al.*[5] Schmid and his co-authors proposed a method that detects and removes hair using global morphological operations and thresholding. They observe that in dermoscopy images hair segments are often thin structures darker than their surroundings. Accordingly, their algorithm starts with transforming the dermoscopy image into the *CIE L*u*v** colorspace and extracting thin structures from its luminosity channel using a morphological closing operation (Fig. 4(c)). It then generates a hair mask by globally thresholding on these thin structures based on their luminosity. At the end, it replaces each masked pixel with an average of its neighboring non-masked pixels via another morphological operation. This algorithm is efficient and the results are good enough for future processing in many cases. It has been adopted by the *DullRazor* hair-removal software[6*]. However, this global approach can sometimes lead to unsatisfactory results. For instance, because the morphological closing operation essentially replaces each hair pixel with its neighborhood average, it can often leave behind undesirable blurring and color bleeding in the result. Moreover, in some dermscopy images (Fig. 4(b), the assumption of hair being darker than the underlying skin and lesion does not always hold, and important dermoscopic features can be mistaken as artifacts and removed. To handle such cases, more explicit hair modelling is required. Fleming *et al.*[5] developed an automated hair detection and tracing algorithm which treats hair as long, relatively straight curvilinear structure with constant width and curvature. This algorithm however, does not model intersecting hair explicitly, so its performance degrades on dermoscopy images containing many hair segments.

To address these issues, we present a novel system that automatically detects artifacts with curvilinear property, i.e. hair and ruler markings, and removes them from dermoscopy images.

- The system performs curve fitting and models curve intersection explicitly to improve accuracy on curvilinear structure detection. This minimizes the chance of removing lesion features accidently.
- The system removes artifacts using exemplar-based inpainting, which preserves underlying lesion features.

Both improved detection accuracy and feature-preserving artifact removal lead to superior results compared to existing techniques. We will describe our approach in the next section.

2. OVERVIEW

Fig. 2 shows the work flow of our approach. The system takes a dermoscopy image as input and generates a luminance difference image[4] to enchance the thin-dark structures present in the image. It then applies Steger's line detection algorithm[7] at multiple scales to extract line segments with certain widths. An intersection analysis algorithm is also applied at this time to reconnect the line segments broken at intersection. Once short segments

[*]In this paper, we use results produced by DullRazor for comparison purpose.

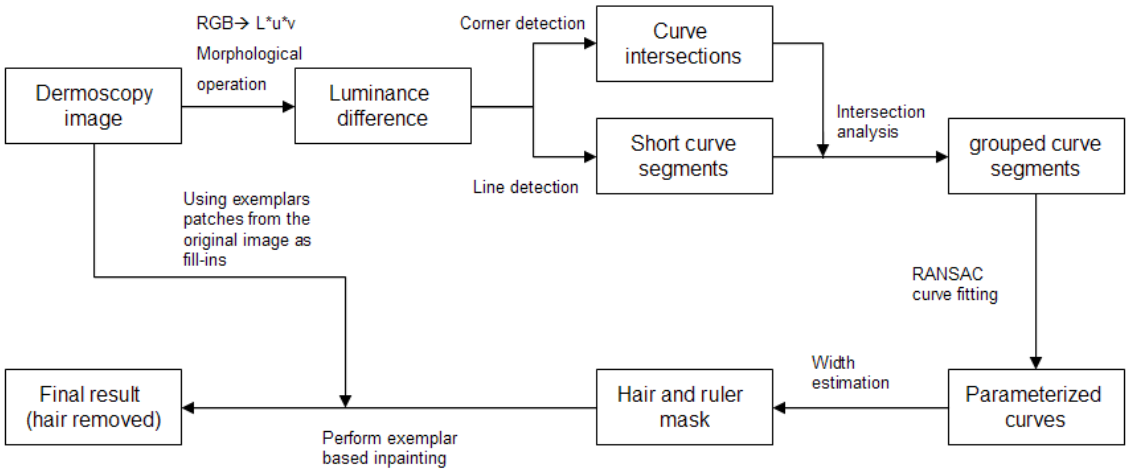

Figure 2. The flowchart describing the work flow of our artifact detection and removal scheme.

are grouped together, the algorithm attempts to robustly fit a curve to each hair segment using RANSAC.[8] Among the good fits, the algorithm accepts long curves, estimates their width, and adds them to the artifact mask. When the mask is complete, it invokes an exemplar-based inpainting procedure[9] to replace the masked sites with its best match from the same image. The replacement patches are selected according to a similarity measure that takes both appearance and feature into account. The procedure stops when all of the artifact pixels are replaced.

3. LINE DETECTION AND CURVE FITTING

3.1 Line points detection and linking

Given a dermoscopy image, we first enhance the thin-dark structures following Schmid *et al.*'s approach.[4] The resulting gray level image (shown in Fig. 4(c) with black/white inverted) is the input for the line points detection step. We adopt the Steger's algorithm[7] to detect line points and link them into line segments. The detection algorithm regards the gray level image as a surface in which pixel intensity corresponds to surface height. The line points are points where the first directional derivative in the direction of the line vanishes and the second directional derivative have a large absolute value. A point (x, y) is a line point if it satisfies $(tn_x, tn_y) \in [-\frac{1}{2}, \frac{1}{2}] \times [-\frac{1}{2}, \frac{1}{2}]$, where (n_x, n_y) is the normalized eigenvector that corresponds to the maximum absolute eigenvalue of the local Hessian matrix $H(x, y)^\dagger$, and t is evaluated as follows:

$$t = -\frac{r_x n_x + r_y n_y}{r_{xx} n_x^2 + 2 r_{xy} n_x n_y + r_{yy} n_y^2}, \tag{1}$$

where $r_x, r_y, r_{xx}, r_{xy}, r_{yy}$ are partial derivatives of the image estimated by convolving the image with discrete two-dimensional Gaussian partial derivative kernels. The standard deviation σ of these kernels is directly tied to the expected line width. Therefore, we apply the line detection algorithm at multiple scales (with different σs) to extract line segments within a certain width range. Fig. 4(d) shows the line points detected from Fig. 4(c). The saliency of a line point (x, y), i.e. the absolute value of the second directional derivative along (n_x, n_y), is inversely proportional to its intensity. After individual line points are identified, we adopt a modified version of Peter Kovesi's [10] linking algorithm to link these points into line segments i.e. sets of ordered points.

$^\dagger(n_x, n_y)$ points to the direction perpendicular to the line direction at point (x, y)

3.2 Curve fitting

As can be seen in Fig. 4(d), the line detection algorithm successfully extracted all the discernable hair segments. However, many thin, dark lesion features were also mistakenly extracted. Since some of these false detection have higher saliency than many true hair segments, thresholding on saliency would not reject the false positives. Moreover, due to image noise and hair color variation, long hair segments are often broken even after the line linking step. This renders thresholding on curve length ineffective too. We observe that individual hairs in most dermoscopy images appear as long, relatively straight curvilinear structures with constant width and slowly varying curvature.[5] In order to reduce false detections, we attempt to fit a curve to each line segment using the least square method.[11] This initial curve fitting step serves mainly as a pre-screener to reject clearly non-hair like structures, i.e. short segments or curves with very high curvature. Let a line segment be given by an ordered set of n points $P_i = (x_i, y_i)$, $i = 1, 2, \ldots, n$. Because the curves we are going to fit tend to be straight, we use the power basis expression for a Bézier curve $B(t) = (B_x(t), B_y(t))$

$$\begin{cases} B_x(t) = a_x t^3 + b_x t^2 + c_x t + d_x \\ B_y(t) = a_y t^3 + b_y t^2 + c_y t + d_y, \quad 0 \le t \le 1. \end{cases} \tag{2}$$

For each given line point $P_i = (x_i, y_i)$, its corresponding parameter value t_i in the Bézier curve power basis expression $B(t_i) = (B_x(t_i), B_y(t_i))$ is calculated using a cord-length parametrization

$$t_i = \begin{cases} 0 & i = 1, \\ \dfrac{\text{length of polygonal line } P_1 P_2 \ldots P_i}{\text{length of polygonal line } P_1 P_2 \ldots P_n} & 1 \le i \le n. \end{cases} \tag{3}$$

The squared sum S of the distances between P_is and their corresponding points $B(t_i)$s on the curve is computed as

$$S = \sum_{i=1}^{n} (\text{distance between } B(t_i) \text{ and } P_i)^2 \tag{4}$$

$$= \sum_{i=1}^{n} (a_x t^3 + b_x t^2 + c_x t + d_x - x_i)^2 + \sum_{i=1}^{n} (a_y t^3 + b_y t^2 + c_y t + d_y - y_i)^2. \tag{5}$$

By setting the partial derivative with respect to each coefficient to zero, we obtain the following system of linear equations for x_i and likewise for y_i. We solve these systems using Gaussian elimination and find coefficients a_x, b_x, c_x, d_x, a_y, b_y, c_y, and d_y that minimize S

$$\begin{cases} a_x \sum_{i=1}^{n} t_i^6 + b_x \sum_{i=1}^{n} t_i^5 + c_x \sum_{i=1}^{n} t_i^4 + d_x \sum_{i=1}^{n} t_i^3 &= \sum_{i=1}^{n} x_i t_i^3 \\ a_x \sum_{i=1}^{n} t_i^5 + b_x \sum_{i=1}^{n} t_i^4 + c_x \sum_{i=1}^{n} t_i^3 + d_x \sum_{i=1}^{n} t_i^2 &= \sum_{i=1}^{n} x_i t_i^2 \\ a_x \sum_{i=1}^{n} t_i^4 + b_x \sum_{i=1}^{n} t_i^3 + c_x \sum_{i=1}^{n} t_i^2 + d_x \sum_{i=1}^{n} t_i^1 &= \sum_{i=1}^{n} x_i t_i \\ a_x \sum_{i=1}^{n} t_i^3 + b_x \sum_{i=1}^{n} t_i^2 + c_x \sum_{i=1}^{n} t_i^1 + d_x n &= \sum_{i=1}^{n} x_i. \end{cases} \tag{6}$$

For robustness, we employ the RANSAC[8] algorithm during the curve fitting step.

3.3 Linking line segments

In dermoscopy images, hair often appear as long curvilinear structure with relatively constant curvature. Therefore, it is more desirable to model it as a single lone segment rather than a train of short segments. Due to image noise, however, the line point linking step often fails to deliver the former. A further line segment linking step is necessary for improved robustness and detection accuracy. Fitting a curve to each line segments not only rejects non-hair like structures, it also facilitates this next step. Fig. 3(a) shows a portion of a dermoscopy images with

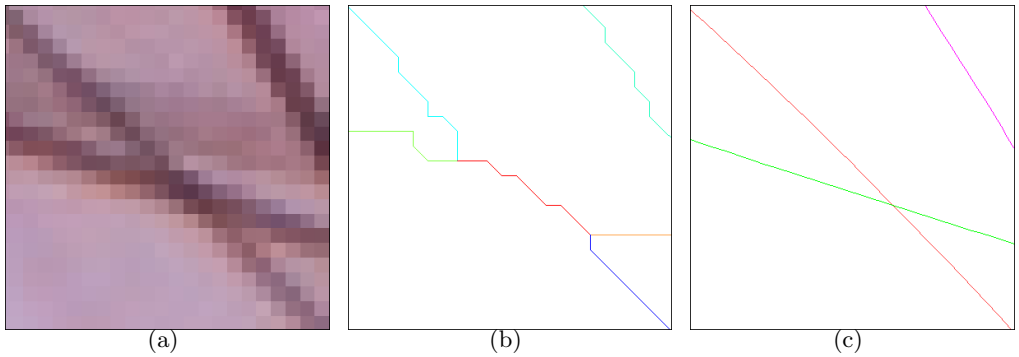

(a) (b) (c)

Figure 3. Linking line segments at hair-hair intersections. (a) A close-up view at a hair-hair intersection. (b) Line segments extracted after the line point linking step. (c) Parametric curves resulted from the intersection analysis and line segment linking step.

hair artifacts. The line segments extracted after the line point linking step is shown in Fig. 3(b). Notice that the green-orange pair of line segments come from the same piece of hair, but it would be difficult for a computer algorithm to detect by just looking at the ends of these line segments. The robust curve fitting procedure, on the other hand, rejects line points that are outliers. The resulting parametric curve not only assumes sub-pixel precision but also has more accurate tangents at possible connecting sites. As a result, our algorithm can then perform windowed searches to identify curve pairs having ends *meet* (within a close vicinity of each other) and reconnect the pairs with matching tangents at the ends. Fig. 3(a) shows a scenario where the linking procedure described above is not suitable. Two hairs intersect each other at a sharp angle, resulting several broken lines and an odd segment in the middle shared by both hairs (Fig. 3(b)). There are a number intersection configurations like this that can lead to inaccurately linked line segments. Our algorithm detects such intersections by identifying special junction segments such as the red segment in Fig. 3(b). It then looks up to a number of common configurations for the best way to pair up the involved line segments, i.e. green-red-orange and blue-red-cyan in this case. At the end, these pairs of segments are linked and refit. Fig. 3(c) shows the parametric curves resulted from this intersection analysis and line segment linking step.

Having a parametric form for each hair also simplifies its width estimation. At each point along the hair, the width can be calculated by measuring the distance between the two foothills of the pixel intensity profile in the normal direction of the curve. Since hair width mostly stays constant in dermoscopy images, we need only estimate the width at one point on the hair, i.e. the most salient line point. In practice, we take an average along each hair to improve robustness. After obtaining the parametric form and width of each hair, we generate an artifact mask to mark the pixels to be removed from the original dermoscopy image.

4. EXEMPLAR-BASED INPAINTING FOR ARTIFACT REMOVAL

Previous works[4] replaces each artifact pixel with the average of its non-artifact neighbors. This approach often leaves behind undesirable blurring and color bleeding(Fig. 5(c)), which may interfere with analytic procedures required for computer-aided diagnosis. To address this issue, we adopt the exemplar-based inpainting and patch-ordering mechanism developed by Criminisi *et al.*[9] At each iteration of the inpainting process, the target patch to be replaced is selected according to a priority term composed of a confidence and a data term defined at every pixel. The confidence term measures how certain a pixel is an non-artifact pixel; this is computed from the confidence of surrounding non-artifact pixels, or artifact pixels that have been already replaced. The data term captures the *strength of flow* of an edge at each pixel on the artifact region boundary. The confidence term enforces that patches containing less artifacts are filled in first while the data term propagates prominent image structures, i.e. edges, in the filling direction. The target patch selected according to this patch-ordering mechanism is then replaced with a source patch found in the original image. The source patch is chosen to minimize the sum squared error (SSE) from corresponding non-artifact pixels in both patches. This exemplar-based approach with a fill-in ordering dictated by image structure ensures that missing morphological features

inside artifact regions are replaced with already existing features from the same image in a systematic way. Our procedure stops when all artifact pixels are replaced.

5. RESULTS

We tested our algorithms on a data set of 460 dermoscopy images. These images are of various qualities. About one eighth of the images have visible artifacts. Our algorithm automatically detects these visible artifacts and removes them. Fig. 4 shows a side-by-side comparison between the artifacts detection and removal results generated by Schmid et al.'s and our method, respectively. Notice that in Schmid et al.'s hair detection result (Fig. 4(b)), although most of the pixels associated with hairs or ruler markings are picked up, a few non-artifact pixels are falsely selected as well due to their dark appearance. We point out that these false detections cannot be avoided by lowering the threshold, because the colors of the skin pigments are almost identical to the hairs. With explicit hair shape modelling, our algorithm successfully detects the hair pixels and rejects dark skin pigments. Fig. 4(f) and 4(e) show artifacts removal results generated by Schmid et al.'s algorithm and ours, respectively. While most of the noticeable hair pixels are removed from both images, the result generated by Schmid et al.'s algorithm has a noticeable blurred appearance at many removed pixel sites. This is due to the interpolation nature of their algorithm. The image generated by our method is free of such artifacts. Upon closer examination of both results (Fig. 5(c) and 5(b)) and the same portion of the original image (Fig. 5(a)), The difference is visible, our algorithm produces results that better preserve the appearance of the original feature. Fig. 6 shows some additional results, ranging from a few isolated hair segments to hairs with many intersections.

6. CONCLUSION

Artifact removal is an important pre-processing step for computer aided diagnosis of pigmented skin lesions from dermoscopy images. In this paper, we present a novel artifact detection and removal scheme. We achieve automatic hair and ruler marking detection using curvilinear structure analysis, and we perform explicit curve fitting to increase the robustness of our detection algorithm. After the artifact pixels are selected, we replace them using feature guided, exemplar-based inpainting. This allows our method to better preserve morphological features that are important to diagnosis. We tested our algorithm on a data set of 460 dermscopy images and the results are promising; our method produces visually superior restoration in comparison to existing techniques.

ACKNOWLEDGMENTS

The authors would like to thank Tim Lee for making DullRazor publicly available on the Web.

REFERENCES

1. D. Rigel, R. Friedman, and A. Kopf, "The incidence of malignant melanoma in the united states: Issues as we approach the 21st century," *J Am Acad Dermatol.* **34**, pp. 839–847, 1996.
2. C. Grana, R. Cucchiara, G. Pellacani, and S. Seidenari, "Line detection and texture characterization of network patterns," in *Proc. of Intl. Conf. on Pattern Recognition (ICPR)*, pp. 275–278, IEEE Computer Society, (Washington, DC, USA), 2006.
3. M. Fleming, C. Steger, A. B. Cognetta, and J. Zhang, "Analysis of the network pattern in dermatoscopic images," *Skin Research and Technology* (5), pp. 42–48, 1999.
4. P. Schmid-Saugeona, J. Guillodb, and J.-P. Thiran, "Towards a computer-aided diagnosis system for pigmented skin lesions," *Computerized Medical Imaging and Graphics* **27**, pp. 65–78, 2003.
5. M. Fleming, C. Steger, J. Zhang, J. Gao, A. Cognetta, I. Pollak, and C. Dyer, "Techniques for a structural analysis of dermatoscopic imagery," *Computerized Medical Imaging and Graphics* **22**(5), pp. 375–389, 1998.
6. T. Lee, "Dullrazor." British Columbia Cancer Agency.
7. C. Steger, "An unbiased detector of curvilinear structures," *IEEE Trans. Pattern Anal. Machine Intell.* **20**(2), pp. 113–125, 1998.
8. M. A. Fischler and R. C. Bolles, "Random sample consensus: a paradigm for model fitting with applications to image analysis and automated cartography," pp. 726–740, 1987.

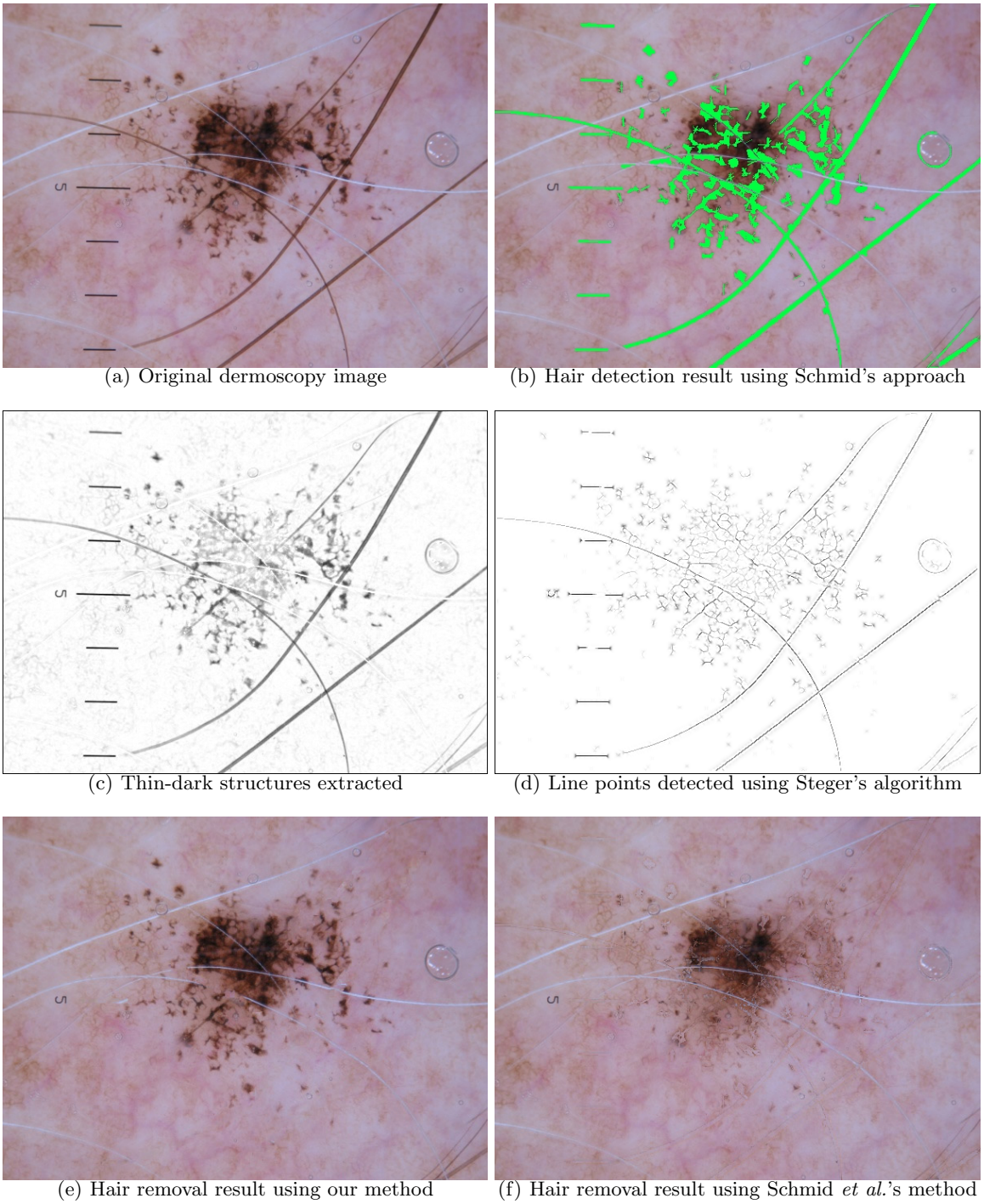

(a) Original dermoscopy image

(b) Hair detection result using Schmid's approach

(c) Thin-dark structures extracted

(d) Line points detected using Steger's algorithm

(e) Hair removal result using our method

(f) Hair removal result using Schmid *et al.*'s method

Figure 4. A side-by-side comparison between the results obtained using ours algorithm and Schmid et al.'s algorithm.

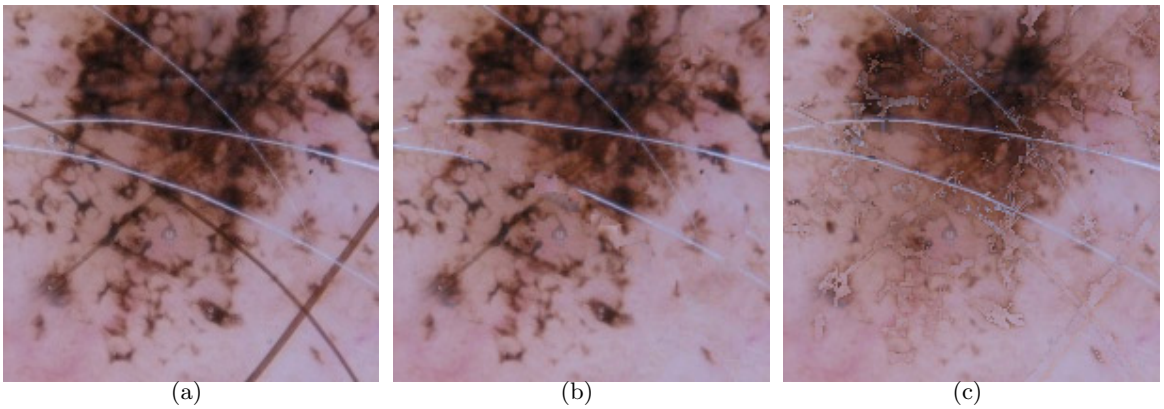

(a) (b) (c)

Figure 5. Close-up views of images from the result comparison in Fig. 4. (a) Original dermoscopy images. (b) Result from using our feature-preserving artifact removal method. (c) Result from using Schmid *et al.*'s method.

9. A. Criminisi, P. Pérez, and K. Toyama, "Object removal by exemplar-based inpainting," in *CVPR*, **2**, pp. 721–728, (Madison, WI), June 2003.
10. P. D. Kovesi, "Matlab and octave functions for computer vision and image processing." School of Computer Science & Software Engineering, The University of Western Australia. Available from: <http://www.csse.uwa.edu.au/∼pk/research/matlabfns/>.
11. K. Itoh and Y. Ohno, "A curve fitting algorithm for character fonts," *Electronic Publishing - Origination, Dissemination, and Design* **6**(3), pp. 195–205, 1993.

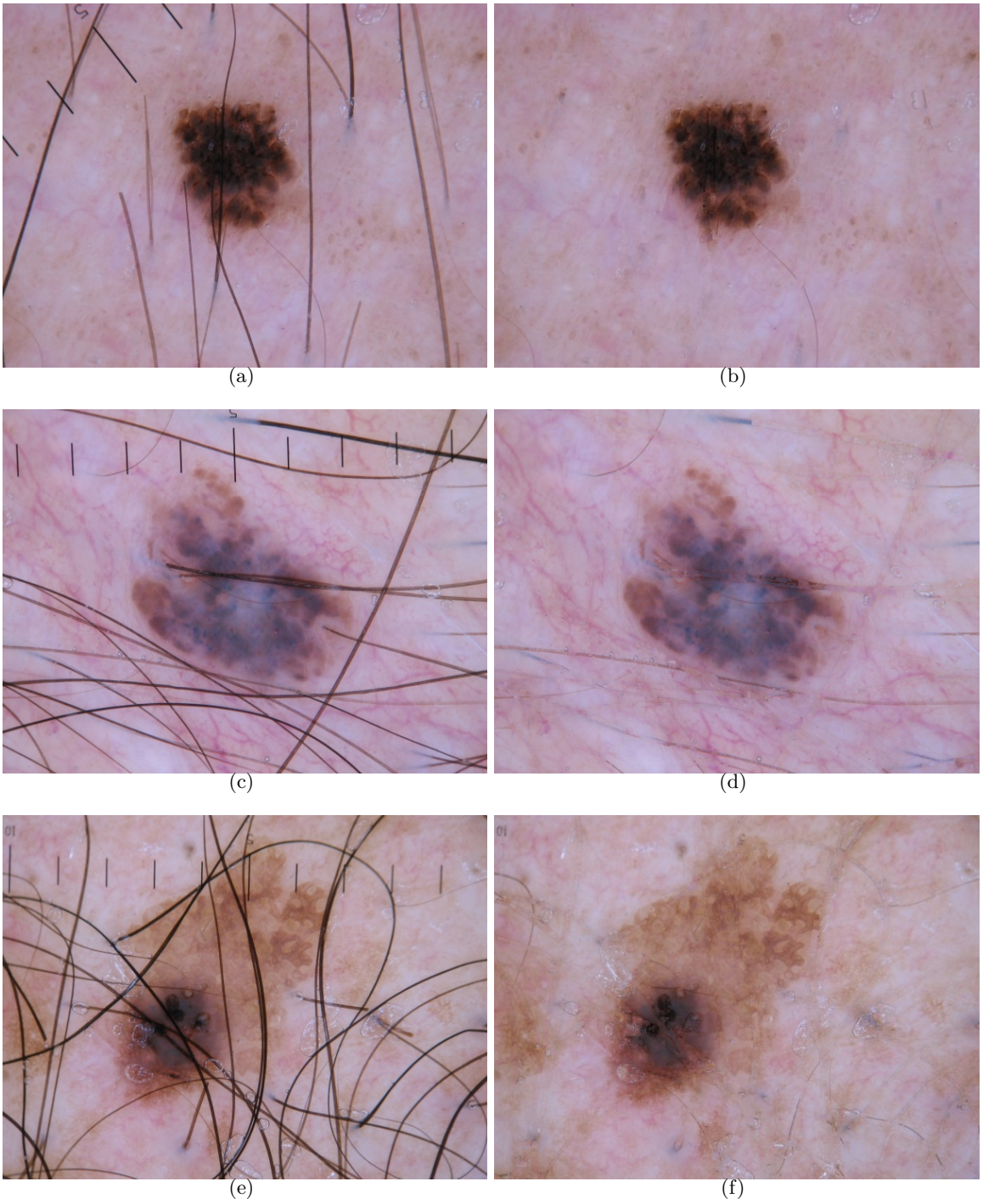

Figure 6. Additional results. (a), (c), and (e) Original dermoscopy images. (b), (d), and (f) Results after performing feature-preserving artifact removal.